Enhancement of microbial fuel cell efficiency by incorporation of graphene oxide and functionalized graphene oxide in sulfonated polyethersulfone membrane

Mehri Shabani, H. Younesi, Maxime Pontié, A. Rahimpour, M. Rahimnejad, Hanxiao Guo, Anthony Szymczyk

Enhancement of microbial fuel cell efficiency by incorporation of graphene oxide and functionalized graphene oxide in sulfonated polyethersulfone membrane

Mehri Shabani[a,b,c], Habibollah Younesi[a*], Maxime Pontié[c], Ahmad Rahimpour[d], Mostafa Rahimnejad[e], Hanxiao Guo[f], Anthony Szymczyk[f]

[a] Department of Environmental Science, Faculty of Natural Resources, Tarbiat Modares University, Imam Reza Street, Noor, Iran, P.O. Box: 46414-356

[b] ESAIP La Salle, CERADE, 18, rue du 8 mai 1945, Saint-Barthélemy d'Anjou Cedex 49180, France

[c] Angers University, Group Analysis & Processes, 2 Bd. Lavoisier, F-49045 Angers 01, France,

[d] Department of Chemical Engineering, Babol Noshirvani University of Technology, Shariati Ave., Babol, Iran

[e] Biotechnology Research Lab., Faculty of Chemical Engineering, Babol Noshirvani University of Technology, Babol, Iran

[f] Universite de Rennes 1, CNRS, ISCR – UMR 6226, F-35000 Rennes, France

Corresponding author: Habibollah Younesi (email address: hunesi@modares.ac.ir)

Abstract

The present work examines, for the first time, the use of thiolated graphene oxide (TGO), in polyelectrolyte composite membranes as an effective approach to enhance the MFC performance. A new composite membrane based on a sulfonated polyethersulfone (SPES) hybrid with GO, sulfonated GO (SGO), and TGO was fabricated and assessed in MFC. The blend membranes were characterized with various techniques. The sulfhydryl (-SH) and sulfonic ($-SO_3H$) groups enhanced the proton selectivity of the membrane and MFC

performance. The MFC using the SPES/SGO1.8% composite membrane generated a power density of 66.4 mW/m^2 which was double that produced by MFC using Nafion117 membrane in batch mode which lasted for 8 days. The SPES/SGO membrane was more selective towards H^+ rather than other cations (K^+, Na^+, and Li^+). This was also confirmed by the results of proton conductivity analysis, as the SPES/SGO1.8% membranes showed a value of 1.42 mS/cm which was higher than Nafion117 (1.3 mS/cm), SPES/TGO1.8% (1.25 mS/cm), SPES/GO1.8% (0.56 mS/cm), and SPES (0.32 mS/cm). The higher COD removal and coulombic efficiency were obtained in MFC with SPES/SGO membranes. In conclusion, it is our view that the new SPES/SGO and SPES/TGO membranes can be applied favorably in dual-chamber MFCs meeting their needs.

Keywords: Microbial fuel cell; Functionalized GO; Proton exchange membranes; Electricity generation

1. Introduction

During the last decades, the depletion of fuel resources and a global movement toward a more sustainable future, have encouraged researchers to seek technologies combined with a renewable energy approach. One of the promising approaches is to try to extract energy and material from waste and wastewater. Among the bio-based methods, bioelectrochemical systems have attracted interest due to their potential in the generation of clean energy. A microbial fuel cell is a type of bioelectrochemical system that utilizes microorganisms to treat the wastewater simultaneously with electricity generation [1]. This is the field of study that deals with harvesting clean energy from waste, which receives growing appeals for its eco-friendly approach and promising efficiency. There are different types of MFC as dual-chamber, single-chamber, wetland, soil MFC, etc. [2–4]. Generally, in a dual-chamber MFC, membranes are placed between two compartments of anode and cathode, and are responsible for physical separation, avoiding the substrate and oxygen crossover, as well as facilitating

the proton transport. There are various types of separators used in MFCs including anion exchange membrane (AEM), cation exchange membrane (CEM), and bipolar membranes [5–9]. For decades, Nafion© has been among the most popular commercially used CEM for the bioelectrochemical system, which provides the transportation of protons and other cations. It contains the negatively charged sulfonated group which defines its high proton conductivity at the same time with an undesirable affinity for other cations as well that cause a pH imbalance [10]. Additionally, Nafion© associates with other limitations as high price ($1500 m^{-2}), substrate loss as well as oxygen leakage [11]. Unfortunately, oxygen crossover may decrease the coulombic efficiency and result in lower power density and inaccurate measurement.

The MFC field is maturing, with a wealth of well-understood methods and ongoing research. One of the main issues concerning the potential use of a dual-chamber MFC is the desirable separation of two compartments. The membrane investigation has met with great success in many aspects [11–13], but there are still many options to consider to replace the commercial Nafion© and overcome its previously mentioned limitations [14–16]. The authors have conducted a comprehensive review of the PEMs applied in a dual-chamber MFC during the last 12 years [5], which provides the team with a strong background to continue the research on the membranes. We have also developed a sulfonated polyether ether ketone/graphene oxide (SPEEK/GO) membrane in an MFC as a PEM [17].

One approach to investigating the alternative material for developing novel membranes is to employ the functionalized polymers either alone [18–20] or by combining with other polymers [21–23] or nanoparticles [21,24] like SiO_2 [25], TiO_2 [26], GO [27,28], metal-organic framework [29], etc.

Among these materials, Graphene oxide (GO) has attracted attention due to its significant characteristics which allow researchers to utilize it in membrane structure. GO is a two-dimensional nano-sheet functionalized carbon-structured material, the functionalized groups

allow its better interaction with a polymer matrix [30]. This material could even become more of interest by grafting other nucleophilic species having nitrogen and sulfur [25,31–35]. The negatively charged structure of GO matches desirably with its application in the formation of CEMs incorporating aromatic ionomers such as SPEEK, SPES, SPS [36–39]. Functionalization of GO is of great importance due to its better synergic mechanism with polymers, and even higher solubility in casting solution [40] as inorganic fillers. Sulfonated GO (SGO) is one of the GO derivatives which is functionalized with sulfonic groups (SO_3^-). This provides GO with proton-conducting channels in the membrane matrix to enhance efficiency as well as the ion exchange capacity [41]. Recently, the SGO was applied as fillers in sulfonated poly(arylene ether sulfone) membranes and resulted in an efficient proton conductivity of the composite membranes and high physical stability [42].

Another functionalized form of GO is via the thiolation (TGO), which means adding the -SH groups to the structure of GO, this is also an approach to establish the negatively charged channels facilitating the proton transport. A thiol functionalized reduced GO (TrGO) was synthesized by refluxing GO with phosphorus pentasulfide as a novel base material for graphene-nanoparticle hybrid materials [43]. Recently, TrGO developed as an efficient ion-to-electron transducing layer for durable solid-contact ion-selective electrodes [44].

In the current paper, we have developed novel membranes based on the incorporation of GO and its functionalized form (SGO and TGO) into the sulfonated polyethersulfone polymer matrix. This research addresses the need for developing some cost-effective, proton-selective, conductive, and efficient membranes that could alternate the use of commercial membranes in an MFC. As far as we know, no previous research has compared the various functionalized forms of sulfonated and thiolated GO in terms of their suitability to be used in the structure of a PEM, as well as their first application in an MFC. With this aim in mind, in this paper we present a full comparison of the as-synthesized membranes through the characterizations including water uptake, cation exchange capacity (CEC), transference number, contact angle,

zeta potential, proton conductivity, and morphological studies, we also compared the result with the commercially available membrane of Nafion117©.

2. Material and methods

2.1. Chemicals

Polyethersulfone (PES Ultrason E6020P with MW = 58000 g/mol) was supplied by BASF Company. Sulfuric acid (H_2SO_4), hydrochloric acid (HCl), chlorosulfonic acid (CSA), dimethylformamide (DMF), and dimethylacetamide (DMAc), sodium hydroxide (NaOH), sodium chloride (NaCl), potassium chloride (KCl), Lithium chloride (LiCl), sodium nitrite ($NaNO_2$), phosphorus pentasulfide (P_4S_{10}), and Natural graphite powder (Gr) were purchased from Merck KGaA (Darmstadt, Germany) and they were used as received without further purification.

2.2. Sulfonation of PES

The sulfonation process of PES was carried out using chlorosulfonic acid (CSA) and sulfuric acid according to the method explained by *Guan et al*., [45]. Firstly, 5 g of PES (previously dried in an oven at 70°C for 6 hours) was dissolved in 50 ml sulfuric acid (solvent) and stirred for 5 hours to obtain a homogeneous solution. Then, the CSA was added dropwise and carefully under vigorous mechanical stirring (250 rpm). The stirring continued for another 3 hours and then the solution was precipitated in an ice-water bath. The precipitate was filtered and washed several times to achieve a neutral pH. Finally, the white-colored noodle-type precipitate was dried overnight in a vacuum oven at 70°C to obtain the sulfonated polyethersulfone (SPES).

2.3. Synthesis of GO, SGO, and TGO and characterization

The GO was prepared according to the modified Hummer's method [46] from pristine graphite. The details are provided in our previous study [17]. The sulfonation process was carried by the addition of a defined amount of the GO into 8 mL of 0.6 M sulfuric acid solution at 70°C. Under continuous stirring, 2 mL of 0.06 M $NaNO_2$ solution was added dropwise and kept at 70°C for 12 h. After the reaction, the solid part was collected by filtration and washed with deionized water (DI) several times until the pH became neutral. The SGO was then oven-dried at 70°C for 24 h [38]. The next functionalizing was conducted through the thiolation. In this process, the GO was reduced through reflux by phosphorus pentasulfide (P_4S_{10}) [43]. We have followed the method explained by *Pham et al*., 2013 [43] with some modifications as follows: first 100 mg of GO was sonicated (Elma, 120H) in 100 ml solvent of DMF for 20 min. P_4S_{10} was then added gradually to the homogeneous solution under nitrogen gas purging. The solution was then continued to be stirred for 12 hours at 120°C. The precipitate was filtered and washed with DI water and ethanol until neutral pH, the TGO was finally left to be dried in a vacuum oven at 70°C for 20h. This is noteworthy to mention that authors have previously fully characterized the GO [17], Here we just display the Fourier transform infrared spectroscopy (FTIR) to estimates the major functional groups of synthesized GO, SGO, and TGO.

2.4. Fabrication of membranes

The cation exchange membranes (CEMs) were prepared using the solution casting followed by the solvent evaporation technique [47]. Generally, there are negatively charged groups, such as $-SO_3^-$, $-COO^-$, $-PO_3^{2-}$ or $-PO_3H^-$, fixed to the membrane backbone of CEMs, enabling them for a selective permeability to the cations [48]. Firstly, various contents (see Table 1) of GO, SGO, and TGO were dispersed in DMAc and sonicated for 20 min, followed by 4 hours of stirring. Then, the SPES (20 wt%) was added to the mixture and continued stirring for another 12 hours to obtain a 20% homogenous solution. Table 1 introduces the composition

of the casting solution to fabricate the composite SPES membranes. After being well mixed, the casting solutions were degassed to remove the bubbles. The casting was carried out by a homemade casting knife with a thickness of 200 microns on flat glass plates. Finally, the membranes were dried at 70°C in an oven for 12 hours and annealing at 100°C for 8 h. After cooling down to ambient temperature, the membranes were peeled off from the glass by immersing it into the DI water bath.

Table 1. The ratio of membrane components used in the membrane structure

Membrane	Composition (wt.%)		
	SPES	GO	DMAc
SPES/GO0.6%	20	0.6	79.4
SPES/GO1.2%	20	1.2	78.8
SPES/GO1.8%	20	1.8	78.2
SPES/SGO0.6%	20	0.6	79.4
SPES/SGO1.2%	20	1.2	78.8
SPES/SGO1.8%	20	1.8	78.2
SPES/TGO0.6%	20	0.6	79.4
SPES/TGO1.2%	20	1.2	78.8
SPES/TGO1.8%	20	1.8	78.2

2.5. Characterization techniques

The chemical structure of GO, SGO, and TGO nanoparticles were analyzed with the Fourier transform infrared spectroscopy (Thermo Nicolet Avatar FTIR 380, USA) in the range between 400 and 4000 cm^{-1}. The elemental analyses of nanoparticles were carried out with a Thermo Finnigan CHNS Analyzer model Eager 300 for EA1112. Before elemental analysis, all samples were vigorously washed many times. The membranes were also characterized by ATR-FTIR spectroscopy, spectrum one (Perkin-Elmer, France), to study their functional groups [49] in presence of SPES. The topography 3D image of the membrane pieces was obtained using an atomic force microscopy setup (Nanoscope III from Bruker, Germany) in contact mode in the air with a scan rate of 1 Hz. The surface and cross-section morphology of samples were conducted by field emission scanning electron microscopy (FESEM-

TESCAN, MIRA III). To prepare the membrane samples for FESEM, they were fractured in the liquid nitrogen and then coated by gold sputter.

2.6. Water uptake, Cationic exchange capacity, and oxygen diffusion coefficient

The presence of water in membrane structure is a key factor for ionic conductivity, however, excessive water uptake (WU) would cause some drawbacks of membrane swelling, reduce mechanical strength which would lead to poor performance [50]. To measure the WU of membrane samples, the methods explained by *Duan et al.*, [51] were implemented. We have first prepared the samples with a surface area of 5 cm^2, then the samples were dried one day in the vacuum oven at 80°C. The dried samples were weighed (W_1) and soaked in DI water for 24 h. Finally, the samples were weighed again (W_2) after careful elimination of excess water. Equation (1) was applied to calculate the WU of membranes.

$$WU\ (\%) = \frac{(W_2 - W_1)}{W_1} \times 100 \qquad (1)$$

We have also applied the acid-base titration method to measure the cation exchange capacity (CEC) of the as-synthesized membrane following the AFNOR method (AFNOR NFX45-200, 2005 [34]). Shortly, the membranes were cut into similar sizes and soaked into 1 M HCl for 24 h, followed by drying in a desiccator for 48 h and weighed. Then, each piece was kept in 50 ml of NaCl (2 M) for 24 h and finally, the titration was conducted using NaOH (0.1 M). The CEC was measured using the following equation, where M and V are the concentration (mg/l) and volume (l) of used NaOH, and W (g) indicates the weight of dried membrane samples.

$$\mathrm{CEC} = \frac{(\mathrm{M}\times\mathrm{V})_{\mathrm{NaOH}}}{\mathrm{W}_{\mathrm{membrane}}} \qquad (2)$$

In the current study, we aimed to provide anaerobic biodegradation of organic load in the anode compartment. To do so, we studied the presence of DO in the anode through the oxygen diffusion coefficient while applying each membrane. All analyses have been

conducted at room temperature around 23±1. The same MFC cell was used while filled with DI water on both sides. The anode side was purged with nitrogen gas till the DO level dropped lower than 0.5 mg/l. The other chamber was aerated continuously. The DO concentration in the anode was followed in 1-h intervals using a DO probe (WTW Multi 3630 IDS, UK) for a total time of 10 hours. Afterward, the oxygen mass transfer coefficient (k_0) (cm/s) and oxygen diffusion coefficient (D_0) (cm^2/s) were determined using the following equations:

$$k_o = \frac{V}{At} ln \frac{c_o - c}{c_o} \quad (3)$$

$$D_0 = k_0 L \quad (4)$$

where c_o and c are saturated DO concentration (mg/l) and DO concentration (mg/l) in the anode at the time t, respectively, V is the anode volume (cm^3), A the surface area of membranes (cm^2), and L the membrane thickness (cm).

In the MFC, it is important to block the oxygen from migrating across the membrane and entering the anodic chamber. Otherwise, the power generated by the MFC drops because the oxygen is being used as electron acceptors by the bacteria rather than by the anode. After all, the former is more thermodynamically favorable [52].

2.7. Proton conductivity (σ)

A high proton conductive membrane is essential for the MFC to improve its ability in generating high power and current. There are two mechanisms where protons follow to pass through the PEMs as a) hopping, and b) vehicular mechanisms (Fig. 1). In the hopping approach, protons hop from a donor hydrolyzed site to an acceptor ionic site without the role of H_2O as carrying molecules (also called Grothuss mechanisms), while in the vehicular system protonated water molecules (H_3O^+) act as carriers of protons through the membrane matrix [53].

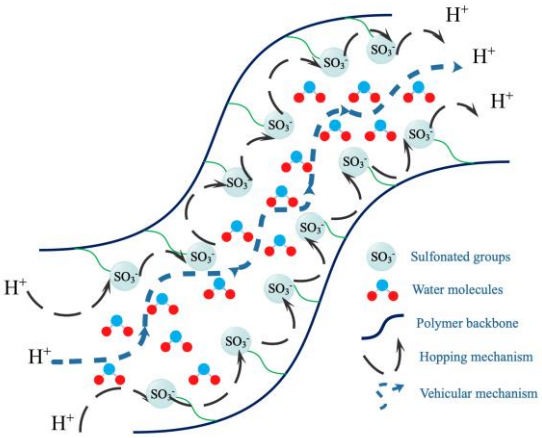

Fig. 1. The schematic of proton transport through the membranes by hopping and vehicular mechanisms

In the present study, the resistance of the membranes was measured using a membrane conductivity test system (MCTS-A1, Iran) over the resistance ranging from 30 mΩ to 30 kΩ at a relative humidity of 100% and room temperature. The composite membranes were the first pre-treated with 1 M H_2SO_4 for 12 h followed by maintaining at DI water for 24 h before analysis. The proton conductivity of the membrane was computed from the resistance data as follows:

$$\sigma = \frac{L}{RA} \quad (5)$$

where, σ is the proton conductivity of the membrane (S/cm), L the membrane thickness (cm), R the ohmic resistance of the membrane (Ω), and A is the membrane surface area (cm^2).

2.8. Membrane transference number (t^+)

To measure the t^+, the method applied by *Tourreuil et al.* [54] was used which principle consists of measuring the potential differences between two solutions of different concentrations, separated by a membrane, here we have chosen the Na^+, K^+, Li^+, and H^+ as the cation with n=1. To conduct the test, a two-compartment cell was applied, one of the compartments (C_1) was maintained at a concentration of 0.001 M targeted electrolyte while the second one (C_2) varies

in concentrations from 0.001 M to 0.01 M. The developed potential differences between the two cells were measured with a digital voltmeter (high entrance impedance of 10 MΩ) using two saturated calomel electrodes (SCE) from Radiometer-Analytical (France). Measurements (3 replicates) were performed 5 min after membrane immersion into the solutions to ensure that a steady state was established. For a charged membrane, and by using the Teorell-Meyer-Sievers model [55], the theoretical membrane potential $(\Delta\phi)_{i=0}$ is expressed by [56]:

$$\Delta\emptyset_{i=0} = E_1 - E_2 = (1 - 2t_m^+)\left(\frac{RT}{nF}\right) ln\frac{c_1}{c_2} \quad (6)$$

where t_m^+ denotes the transport number of the cation electrolyte in the membrane phase. In the present study n = 1 due to the choice of electrolytes. The transference numbers (t_m^+) measured for the different studied membranes have to be compared with the t_m^+ in free solution which is previously reported in the literature review (see Table 5) in the examined concentration range [57].

2.9. Zeta potential

Membrane zeta potential was determined from tangential streaming potential measurements [58,59] using a SurPASS electrokinetic analyzer (Anton Paar GmbH, Graz) equipped with Ag/AgCl electrodes and an adjustable-gap cell. Measurements were conducted at room temperature with 0.001 M potassium chloride (KCl) background solutions in the pH range 3-9 (the pH was adjusted with 0.05 M HCl and potassium hydroxide (KOH) solutions). The distance between the membrane samples was set to 100 ± 5 mm.

2.10. Contact angle

Water contact angles were measured by the sessile drop method using a DIGIDROP GBX-DS apparatus. Contact angle has been used as an index of the wettability of the membrane active layer. Before measurement, membranes were stored in a container of pure water for 24

h at 4 °C. The rinsed membranes were dried in a desiccator before measurement. The samples were vacuum-dried for 72 h before the measurements. Membrane samples were cut into small pieces and mounted in support. An approximately 2.0 µl droplet of pure water was placed on the membrane specimen and the contact angle was measured with the goniometer via the camera immediately after the drop placement. Contact angles were determined using a video capture system and the Windrop^{++} software. The reported contact angles are the average of at least 10 measurements performed at different locations on the membrane surface. Measurements were performed at room temperature.

2.11. MFC design

A dual-chamber MFC with a working volume of 800 mL was built from plexiglass by the authors to follow the analysis [17] (Fig. 2). The anode and cathode compartments were separated by a commercial CEM (Nafion117 (Sigma-Aldrich) versus as-synthesized membranes) with a surface area of 16 cm^2. The carbon cloth (CC) material was used as anode and cathode electrodes (12 cm^2). The anaerobic anode chamber was filled with industrial wastewater and anaerobic mixed bacteria sludge; taken from a sewage treatment plant (Chamestan Industrial Park, Mazandaran, Iran), while the aerobic cathode was only composed of water (The air was purged continuously). The average value from the four replicate analyses with a relative standard deviation (SD) and range values of the wastewater characteristics are provided in Table 2.

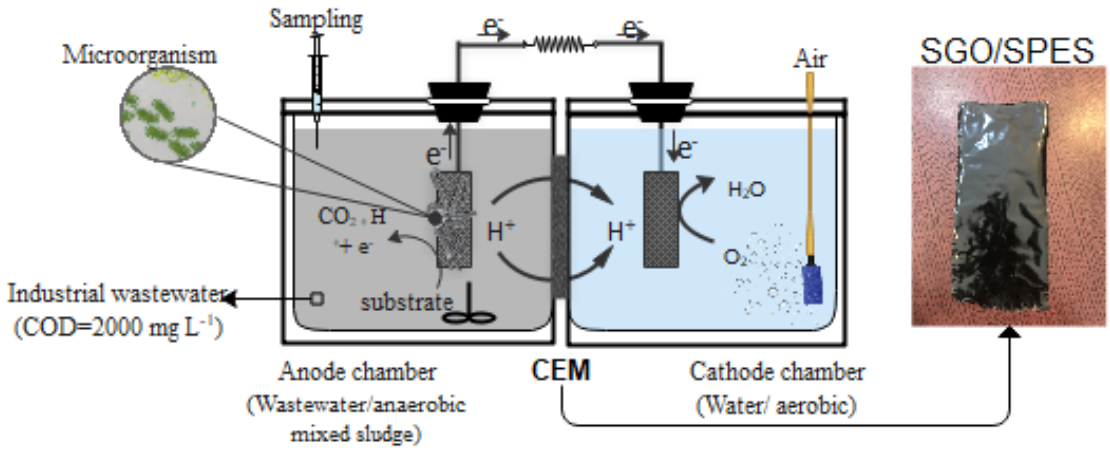

291

292 **Fig. 2.** The schematic of applied dual-chamber MFC

293

294 Before the start of each experiment, the nitrogen (g) was purged for 15 minutes into the
295 anode cell to ensure the anaerobic phase and re-checked daily using a DO probe to maintain
296 the anaerobic condition. The initial chemical oxygen demand (COD) of all systems was
297 around 2000 mg/l. The two electrodes were connected using external resistance-induced
298 wires and connected to an analog/digital data logger (Danesh Gostar Hamgam Ba
299 Sanat Company (Babol, Iran)) and a personal computer (PC) to record the data. The
300 performance of lab-scale MFC under different batch-mode conditions was conducted in terms
301 of COD removal percentage, power production through the polarization curves, and
302 coulombic efficiency. The power and current densities produced by the MFC were measured
303 through the polarization curve following the ohm's law in equations 7-10. All MFCs operated
304 for 7 days at OCV (open circuit voltage) to establish stable voltage and power; the data were
305 recorded from the 2nd day using the analog/digital data logger. Measurements were carried
306 out at variable resistances imposed on the MFC.

307 $$I = \frac{U}{R} \quad (7)$$

308 $$P = U \times I \quad (8)$$

$$PD = \frac{P}{A_{anode}} \quad (9)$$

$$ID = \frac{I}{A_{anode}} \quad (10)$$

where I, R, U, and P are current (A), Resistance (ohm), potential (V), and power (W), respectively. The power density (PD) and current density (ID) are power and current normalized by the anode surface area (A_{anode}).

Table 2. Characteristics of industrial wastewater applied in MFC (Chamestan Industrial Park, Mazandaran, Iran)

Parameters	Average value ± SD	Range value
pH	6.70 ± 0.42	6- 6.9
Total Kjeldahl Nitrogen (TKN), mg/l	21.32 ± 0.55	18.45-22.10
Total dissolved solids (TDS), mg/l	952.43 ± 112.70	900.5-1200
Total suspended solids (TSS), mg/l	2332.14 ± 426.00	2100-3000
Biological oxygen demand (BOD_5), mg/l	820.36 ± 42.00	800-900
Chemical oxygen demand (COD), mg/l	2010± 135.60	1900-2100
Nitrate-N, mg/l	74.88 ± 2.24	70.02-77.30
Phosphate-P, mg/l	10.02 ± 0.31	9.4-10.30

2.12. COD removal and coulombic efficiency

To study the efficiency of MFC in wastewater treatment and bioelectricity generation, the COD removal and coulombic efficiency (CE) were measured and reported in Table 6. The samples were taken from the anode compartment by a syringe at the initial time and repeated every 24 hours. The COD removal efficiency was measured for 7 days, applying the initial (COD_i) and final COD_f (mg/l) as follows:

$$COD\ removal = \frac{COD_i - COD_f}{COD_i} \quad (11)$$

We report CE based on COD changes (equation 12) defined as the fraction of electrons recovered by the current [60]. Generally, the CE could be limited by factors like electron consumption by methanogenesis, oxygen crossover, and aerobic respiration of cathode biofilm [61]. The CE value can be measured using the oxygen molecular weight (*M*, 32 g/mol), Faraday's constant (*F*, 96485 C/mol), number of electrons exchanged per mole of

oxygen (b, 4 mol e^-/mol O_2), the volume (l) of liquid in the anode compartment (v_{An}), and ΔCOD (g/l) over time t:

$$CE = \frac{M \int_0^t I \, dt}{F b v_{An} \Delta COD} \quad (12)$$

3. Results and discussions

3.1. FTIR characterization

Fig. 3 shows the FTIR spectra of GO, SGO, and TGO nanoparticles. The spectrum of GO displays peaks at 3500 cm^{-1}, 1712 cm^{-1}, 1616 cm^{-1}, and 2380 cm^{-1} which corresponds to characteristic bands of stretching vibration of the hydroxyl group (-OH) [32], carboxyl (COO^-), C-C, and C-H band groups, respectively. Also, the peaks observed around 1220 cm^{-1} and 1025 cm^{-1} suggest the presence of O-C stretching and bending modes both in GO and TGO samples [62]. These results support the oxidation of graphite to GO. The details of GO were also reported earlier by authors [17]. The FTIR spectra of SGO present a characteristic peak at 2923 cm^{-1} assigned to the absorption of the sulfonic acid groups (-SO_3H) [63], and a peak that appeared at 1060 cm^{-1} can be attributed to the symmetric stretching vibration of -SO_3H groups [64]. A broad peak presents the stretching vibration of -OH in carboxylic acid and phenol groups ascribed from 3330 cm^{-1} to 3520 cm^{-1}. a weak peak observed at 876 cm^{-1} is referred to as the wagging of hydrogen out-of-plane of SGO rings [64]. During the process of thiolation, we observe the depletion of -OH peak in TGO (around 3500 cm^{-1}), which arises from the conversion reaction of -OH groups to the substituted -SH group. Significant differences were observed in the TGO FTIR spectrum comparing to GO which provided us with the successful thiolation process. Many peaks are assigned to thiol groups and amide bond as: 2615 cm^{-1} (S-H stretching) [32], 1567 cm^{-1} (N-H stretching), 3043 cm^{-1} and 3505 cm^{-1} (N-H bending), 678 cm^{-1} (N-H wagging) [65]. Also, it should be noted that -SH related

354 peaks are difficult to be recognized in FTIR due to the masking that happened by the
355 vibration of many peaks present in the spectrum of GO [33].
356 The ATR-FTIR spectra of SPES and SPES/SGO1.8% within the wavenumber range of 500–
357 4000 cm^{-1} are also depicted in Fig. 3. The ATR–FTIR spectroscopy measurements were
358 conducted to identify the existence of new bonds. The presence of -SO_3H groups in SPES is
359 confirmed by the following peaks at 1740 cm^{-1} and 1635 cm^{-1} ascribed to the vibration of the
360 aromatic skeleton [66]. The two absorption peaks at 1020 cm^{-1} [28] and 1143 cm^{-1} [34]
361 indicate the characteristic symmetric stretching of aromatic –SO_3H groups. The stretching
362 vibration in the range of 3000 cm^{-1} to 3500 cm^{-1} is assigned to O-H stretching absorption.
363 The vibration band at 2170 cm^{-1} for SPES is due to the presence of C=C stretching. Also, the
364 presence of aliphatic C-H bands is observed by the peaks at 2850 cm^{-1} to 2930 cm^{-1}. Due to
365 the overlay of the peaks with SPES, the typical peaks of GO, SGO, and TGO are not easy to
366 be observed in SPES/SGO1.8% membrane [34]. However, the SPES and SPES/SGO1.8%
367 spectra are presented as no difference was observable among the FTIR spectra of SPES/GO,
368 SPES/TGO, and SPES/SGO. Further, by comparing the spectra of both membranes in the
369 range of 500 cm^{-1} to 2500 cm^{-1}, we can observe significant differences indicating the bonds
370 between the SPES and nanoparticle s.

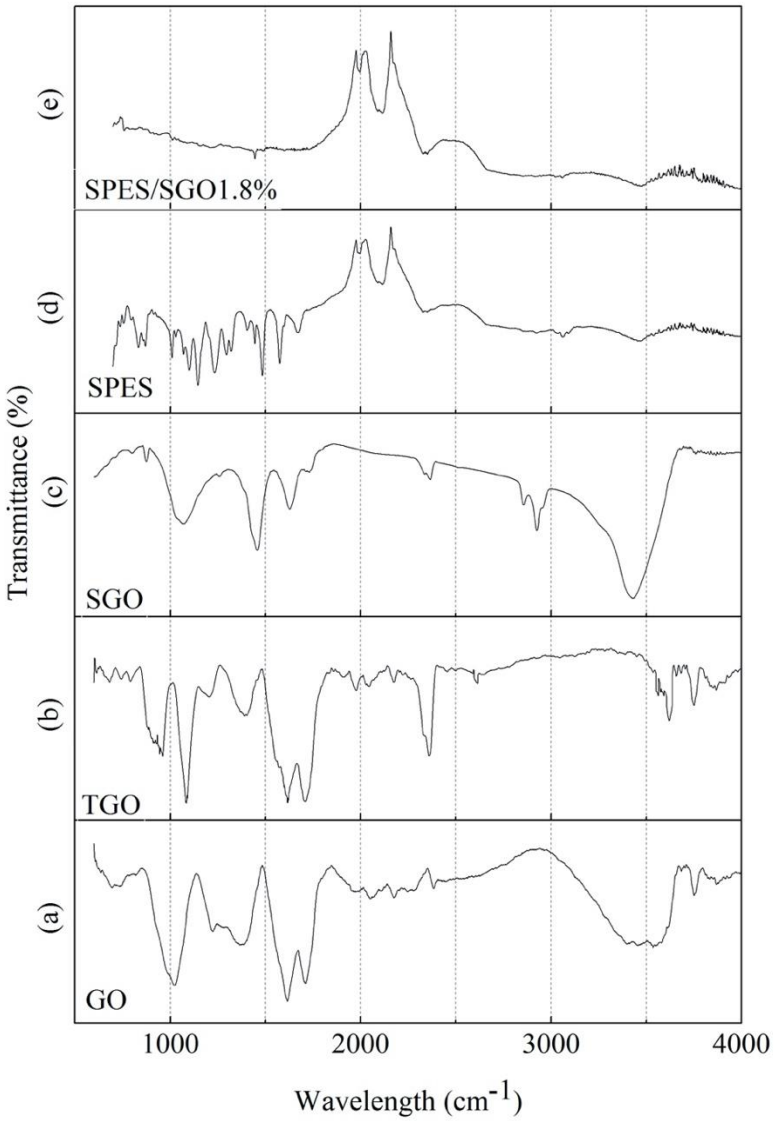

Fig. 3. FTIR spectra of GO, SGO, and TGO, and SPES, SPES/SGO1.8% membrane sample

3.2. Elemental analyses (CHNS)

CHNS is an elemental analysis to accurately determine the concentrations of carbon, sulfur, hydrogen, and nitrogen in organic and inorganic solid samples. Table 3 presented the obtained results for GO, SGO, and TGO. This test aimed to prove the presence of sulfur more in SGO and TGO and compare it with GO samples. Here, GO showed a composition of 45.34% carbon, 0.15% sulfur, while the percentage of sulfur in SGO and TGO has increased to 6.23% and 5.5%, respectively. It Confirms the successful synthesis and presence of -SO_3H and -SH functional groups in functionalized forms of GO. On the other hand, the amount of

oxygen has decreased in SGO and TGO which indicates the introduction of sulfonate and thiol functional groups to oxygenated functional groups in GO and their replacement [35,67–69]. It should be noted that the oxygen content was calculated by subtracting carbon, hydrogen, nitrogen, and sulfur from 100%.

Table 3. CHNS analysis of GO, SGO, and TGO

Element	GO (wt%)	TGO (wt%)	SGO (wt%)
C	45.35	66.32	50.76
H	2.36	1.42	2.1
N	1.86	2.3	2.7
S	0.15	5.5	6.23
O	50.28	24.46	38.21

3.3. Morphology and topography of the membranes

The microstructure of the membranes is one of the main parameters that should be studied because it will provide useful information on the distribution of the nanoparticles, ionic sites, porosity, and integrity. The cross-section morphological structure of the SPES, SPES/GO1.8%, SPES/SGO1.8%, and SPES/TGO1.8% have been observed through cross-sectional SEM images as displayed in Fig. 4. A general look, states that the membranes are greatly affected by the addition of GO, SGO, and TGO. A detailed comparison of images 4a with 4b, c, and d confirms the presence of nanoparticles (NPs) and their distribution in the polymer matrix and not only the surface of the membrane. A better understanding of the GO structure was reported previously [17] using the XRD and SEM morphological analyses, which prove that the single layer of GO, the lower crystallinity of GO, and the presence of amorphous structure occurred during graphite oxidation. Further, the TEM image of GO was displayed to have a characteristic 2D sheet-like structure [17]. However, the FESEM image of GO sheets was layered on the SPES matrix in SPES/GO1.8%, as shown in Fig. 4b. In addition, the SGO nanosheets were dispersed as revealed in Fig. 4c. The SGO nanosheets demonstrate a well curvy and exfoliated overlapped structure leading from hydrophobic –

SO3H groups amendment on the GO surface. Furthermore, the TGO was distributed homogeneously on the SPES matrix in SPES/TGO1.8%, as revealed in Fig. 4d. There is also a significant difference in thickness of the membrane before and after the incorporation of the nanoparticles, where SPES has a dry thickness of 34.3 μm while this value has increased to 60 μm, 100 and 115 μm in SPES/GO, SPES/SGO, and SPES/TGO. This might be due to the addition of NPs which has increased the viscosity of the casting solution resulting in a higher thickness. A similar conclusion was stated that these changes in thickness could be related to casting solution viscosity [70]. The clustering structure of GO and the ionic sites are easily observed through the image 4b, 4d, and especially 4c. The SPES/SGO showed the best clustering and honeycomb structures resulting from the presence of SGO nanoparticles, this is due to the positive effect of sulfonated groups on providing the channels and clusters which lead to facilitated proton transport. This agrees with the earlier study as claimed layered structure can provide facilitate proton conductivity in parallel paths and channels to create more proton transfer and adsorption of more water [34]. Besides, the membranes displayed a dense structure, without visible porosity at the micrometric scale which supports their application in microbial fuel cells and non-porous PEM. The non-porous structure is induced from the preparation method of the solvent evaporation technique.

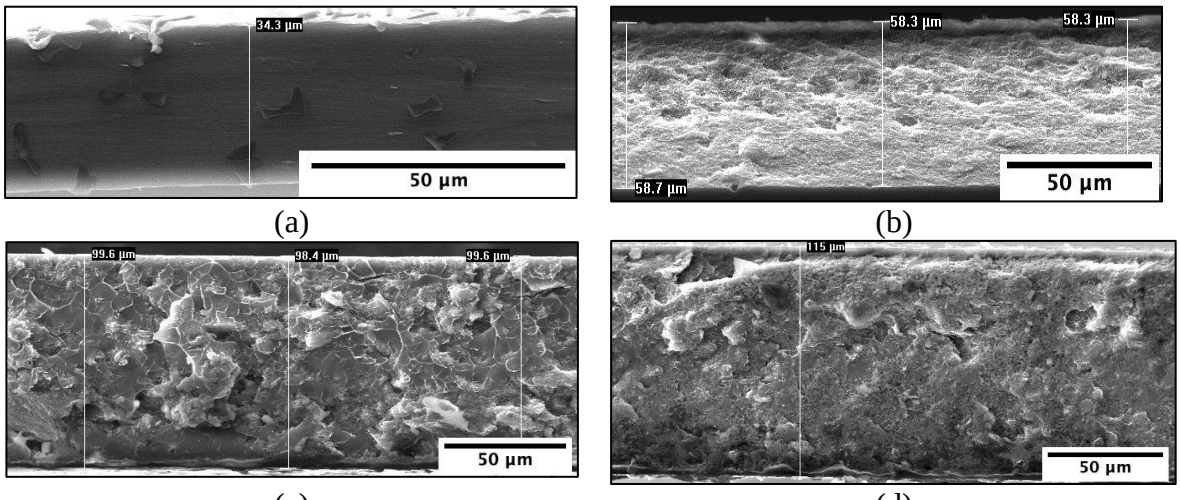

Fig. 4. Cross-sectional images of a) SPES, b) SPES/GO1.8%, c) SPES/SGO1.8%, and d) SPES/TGO1.8%

3.4. Water uptake, contact angle, and diffusion coefficient

In this section, we will illustrate experimental results on water uptake (WU), contact angle (CA), and oxygen diffusion coefficient as listed in Table 4. The effect of the addition of nanoparticles is observed by comparing the value of WU. As presented in Table 4, the WU of the SPES membrane is around 12.33%, which is lower than Nafion117 of 17.5% as the control sample. The incorporation of nanoparticles (GO, SGO, or TGO) improved the WU by the membranes, significantly. within each membrane group, WU increases with increasing the ratio of nanoparticles in the polymer matrix. While $-SO_3^-$ incorporated membranes showed the highest value compared to other functionalized forms with a similar ratio. For example, the SPES/SGO1.8% with the WU of 36.3% presented a higher value than SPES/GO1.8% and SPES/TGO1.8% of 23.1 and 30%. Based on our observation, the WU values higher than 40% causes instability and membrane swelling in contact with 100% humidity atmosphere, this happens due to the high hydrophilicity of the membrane. The results of the WU analysis are then compared with the CA test. The trend showed almost in agreement with the results of CA, indicating the hydrophilicity of the membranes [71]. It is worth discussing this interesting fact revealed by comparison of the PES and SPES membranes. It showed that due to the presence of hydrophobic backbone polymer in PES, it almost absorbed no water. This result ties well with previous studies supporting us with a suitable choice of sulfonation of the bare polymer [45,72].

We also present the results of oxygen diffusion (D_0), which show the permeability of the membrane to the oxygen. In the MFC, we favor the anaerobic degrading anode to provide a suitable condition for microorganism activity and to achieve a higher produced current. This theory has also been followed in earlier studies where they resulted as; the denser the polymer matrix was, the lower the oxygen diffusion became [11,73]. One concern about the Nafion© pointed out in the literature review, was its high oxygen diffusivity [5,15], which is

also the case here. However, the as-synthesized membranes do seem to improve this feature at least 5 times lower. Generally, by increasing the ratio of nanoparticles (from 0.6 to 1.8%) in the polymer matrix, the k_o becomes lower due to the higher density. As shown in equation (3) the membrane thickness is also a crucial factor in measuring the k_o, which was on average 180, 60, 40, 60, 100, 115 mm for Nafion©, PES, SPES, SPES/GO, SPES/SGO, and SPES/TGO, respectively (Fig. 4). In all the membranes, the wt% of 0.6 of nanoparticles was the most unfavorable, while both 1.2% and 1.8% incorporation of nanoparticles brought significant difference comparing to 0.6. This indicated the optimal percentage of incorporation is around 1.8, as the differences from 1.2 to 1.8 are much smaller than 0.6 to 1.2.

Table 4. Water uptake, contact angle, oxygen mass transfer coefficient, and oxygen diffusion coefficient of membranes

Membrane	WU, %	Contact angle, degree	k_o, cm/s	D_o, cm^2/s
Nafion117	17.5	90 [74]	7.29E-04	1.31E-04
PES	5.41	87 [75]	nd	nd
SPES	12.33	90.1	8.50E-04	4.25E-05
SPES/GO0.6%	20.71	90.7	9.81E-04	5.89E05
SPES/GO1.2%	22	84.5	8.82E-04	5.29E-05
SPES/GO1.8%	23.13	64.3	8.50E-04	5.10E-05
SPES/SGO0.6%	28.41	78.7	5.22E-04	5.22E-05
SPES/SGO1.2%	33.54	76.0	4.36E-04	4.36E-05
SPES/SGO1.8%	36.32	78.5	4.26E-04	4.26E-05
SPES/TGO0.6%	24.55	82.2	5.00E-04	5.50E-05
SPES/TGO1.2%	26.22	71.0	4.48E-04	4.93E-05
SPES/TGO1.8%	30	70.9	4.35E-04	4.78E-05

nd = not determined

3.5. Transference number, cation exchange capacity, and proton conductivity

The motion of the ionic species ensures current transport through the electrolyte(s). the transference number (t^+) is a very important parameter giving the current value carried by each ion [76]. In an MFC working with cation exchange membranes, the transport of other cations happens with the protons, sometimes even more than protons. This transport causes

an accumulation in the cathode compartment that results in a large pH difference between the two compartments. The pH imbalance brings some serious drawbacks [77], so in the present study, it was necessary to analyze the novel membranes in terms of various cations transport. Table 5 presents the transference number for four electrolytes of H^+, Na^+, Li^+, and K^+ with chloride as a counter ion. This has been measured from the potential differences for different concentrations of each electrolyte. Considering the literature review, one of the limitations of the Nafion© membrane was its weak selectivity to the protons [10,14], this was also observed in the present study. As the data stated Nafion© has the highest t^+ to the potassium ion followed by Na^+, H^+, and Li^+. A high value of the transference number for K^+ was also reported earlier [78]. Herein, the values show that the Nafion© membrane behaves nearly equal toward the chosen cations. This is the usual order followed by some reported membrane [79–81]. However, the GO functionalized membranes show various trends due to the polymer matrix interaction [82]. In SPES/GO membranes it is obvious that a trend is starting to form but it is still the sodium and potassium ions that showed a higher value of t^+. By increasing the ratio of GO in the membrane matrix, a slight difference from 0.72 to 0.8 has been achieved. The highest H^+ transference number ($t(H^+)$ belongs to SPES/SGO1.8% (0.88) followed by SPES/GO1.8% (0.8), Nafion117 (0.76) and SPES/TGO1.8% (0.73). Among the functionalized nanoparticles, the results proved that groups in SGO have improved the membrane selectivity more efficiently than TGO and GO. We assume this is more due to the synergic effects between groups of both polymer (SPES) and nanoparticles (SGO). In this test, rather than the order of ions (which could be associated with different parameters), the important information to extract is the differences in the value of ion transference number in comparison to the Nafion117. As mentioned, the t^+ in Nafion© for all electrolytes is somehow near to each other while in the synthesized membranes, we could observe increased differences between the electrolytes, indicating the improved selectivity of the proposed membranes.

494

495 **Table 5.** The transference number of H^+, Na^+, Li^+, and K^+ electrolytes for membranes

Membranes	Transference number (t^+)				
	H^+	Na^+	Li^+	K^+	Comparison
SPES/GO0.6%	0.72	0.71	0.62	0.78	$K^+>H^+=Na^+>Li^+$
SPES/GO1.2%	0.73	0.87	0.63	0.86	$Na^+>K^+>H^+>Li^+$
SPES/GO1.8%	0.8	0.82	0.76	0.79	$Na^+>H^+>K^+>Li^+$
SPES/SGO0.6%	0.79	0.58	0.67	0.6	$H^+>Li^+>K^+>Na^+$
SPES/SGO1.2%	0.80	0.62	0.63	0.65	$H^+>K^+>Li^+=Na^+$
SPES/SGO1.8%	0.88	0.67	0.56	0.73	$H^+>K^+>Na^+>Li^+$
SPES/TGO0.6%	0.72	0.68	0.58	0.48	$H^+>Na^+>Li^+>K^+$
SPES/TGO1.2%	0.7	0.6	0.6	0.64	$H^+>K^+>Na^+=Li^+$
SPES/TGO1.8%	0.73	0.59	0.4	0.58	$H^+>Na^+>K^+>Li^+$
Nafion 117-0ld	0.76	0.78	0.71	0.83	$K^+>Na^+>H^+>Li^+$
Free diffusion	0.82	0.39	0.33	0.49	$H^+>K^+>Na^+>Li^+$

496

497 Other promising findings are proton conductivity and cationic exchange capacity as presented
498 in Fig. 5. Among all tested membranes, SPES/SGO1.8% had the highest proton conductivity
499 of 1.42 mS/cm followed by Nafion117 (1.3 mS/cm), while SPES/TGO1.8%, and
500 SPES/SGO1.2% showed slightly lower conductivity around 1.25 mS/cm. According to the
501 data provided, the lowest proton conductivity belongs to the PES membrane which also has
502 the lowest cation exchange capacity. Sulfonating the polymer cause an increase from 0.28
503 mS/cm to 0.36 mS/cm which is still not satisfying, but the addition of nanoparticles provides
504 a significant difference. This is inconsistent with the previous studies that achieved higher
505 values of proton conductivity in the case of sulfonated polyether ether ketone (SPEEK)
506 incorporated with GO [17,83]. The reason is the presence of oxygenated, sulfonated, and
507 thiolated functional groups on the GO that helps to improve the proton conductivity. It is
508 assumed that protons move through the paths and channels provided by the functionalized
509 groups and in their presence. It could simply mean that a network has been formed between
510 these functional groups, ionic sites in SPES, and water molecules, resulting in higher proton
511 diffusion [83]. The values of proton conductivity for TGO type membranes are generally
512 lesser than SGO functionalized membranes indicating the better performance of sulfonation

functionalization. It is important to highlight the fact that cationic exchange capacity values are following the proton conductivity (Fig. 5). So, a membrane with higher CEC showed a higher proton conductivity as well. The order of tested membranes for cationic exchange capacity is as follows: Nafion117~ SPES/SGO1.8%> SPES/TGO1.8%> SPES/GO1.8%> SPES > PES. This was also the case in WU, so the higher the WU, the higher the proton conductivity, because the proton transfer will be much easier when there is a formation of water bonds [25]. Considering the Grotthuss mechanism [53] (Fig. 1), it is believed that proton hopping has happened between different molecular units via the hydrogen bridge by a reoriented motion. In addition to the hopping approach, we assumed that a fraction of protons has also passed through the membrane by the vehicular mechanism due to the membrane WU, fully hydrated atmosphere, and the presence of water molecules in the structure.

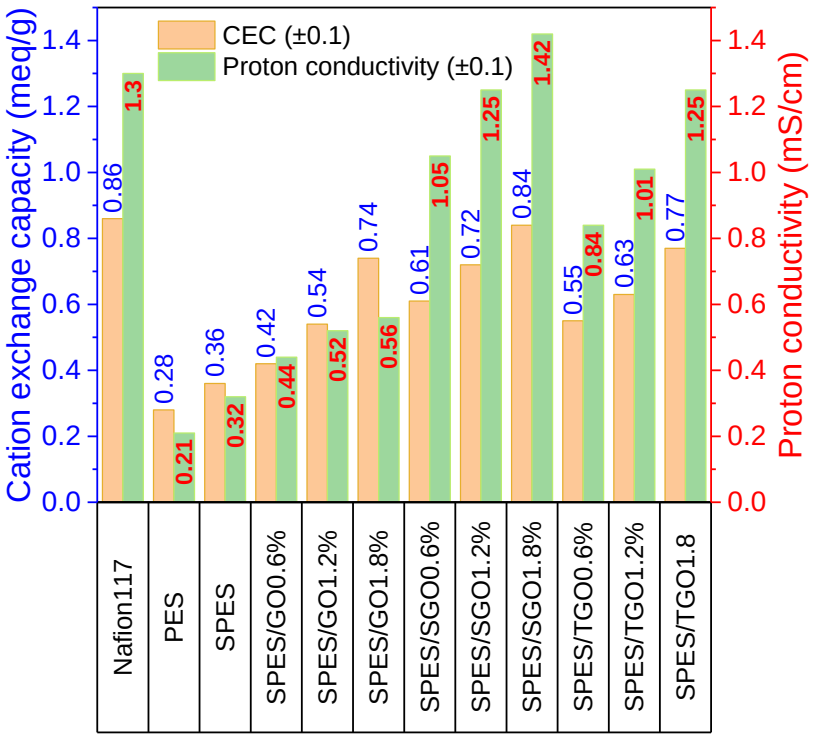

Fig. 5. Cation exchange capacity and proton conductivity of membranes

3.6. Contact angle (CA) and zeta potential of the membranes

The relative hydrophilicity or hydrophobicity of the membrane surface was measured via contact angle (CA). This is the angle formed between three phases of a solid membrane, a liquid water drop, and air (or another gas) [23] and determined from the sessile drop technique. It is well accepted that the lower the contact angle, the higher the hydrophilicity of the surface [84]. The CA of 0° indicates a wetting surface, as CA > 90° a hydrophobic one. While contact angle is commonly used to measure the hydrophobicity of the membrane surface, the data should be used with some caution. In practice it is not an absolute value, it is a relative parameter comparing different material surfaces, i.e. the membrane surface roughness can influence contact angle measurement due to capillary effects, and results from different measurement methods can vary considerably [85]. If roughness is higher than 100 nm, the measured contact angles are meaningless. On very rough surfaces, contact angles are larger than on chemically identical smooth surfaces [86,87].

The CA for all samples was measured and displayed in Table 4. This test aimed to observe the positive effect of nanoparticles on improving the hydrophilicity in the non-porous structure of the SPES membrane. Generally, after the addition of functionalized nanoparticles to the SPES polymer matrix, the contact angles decreased, and a more hydrophilic membrane was fabricated. As shown, the highest contact angle (lowest hydrophilicity) was associated with the SPES membrane at 90.1°. A similar amount was also reported by previous studies [88,89]. They reported that the hydrophilicity of PES membranes was improved by blending with sulfonated PES. In SPES/SGO and SPES/TGO, the CA decreases with the increase of the nanoparticle wt% in the SPES matrix, defining the higher the NPs ratio was the more hydrophilic the surface. SPES/GO0.6% showed the lowest contact angle as 64.3° followed by SPES/TGO1.8% as 70.9°. the order of average hydrophilicity for the -GO, -SGO, and -TGO functionalized membranes are as followed:

SPES/TGO> SPES/SGO> SPES/GO

As proved by the result, all the synthesized membranes have a lower CA than Nafion117 reported in the literature review. A study reported that incorporation of GO and TiO_2 into the Nafion© improves the contact angle from 89.8° to 68.6°and 71.2 [90] resulting in a more hydrophilic surface. It is also stated that GO is more hydrophilic than TiO_2 supporting our choice of nanoparticles. For SPES/SGO1.8% due to its relative hydrophilic structure, it could be less sensitive to biofouling vs more hydrophobic membranes of SPES or Nafion© [91]. Earlier it has also been stated that membranes with GO have better anti-biofouling properties [92].

Another parameter we focused on was zeta potential, which is applied for measuring the surface charge characteristics of the as-synthesized polymeric membranes. The results of zeta potential values under different pH are displayed in Fig. 6. This value is also in relation to the ion-transport selectivity by partitioning of multivalent ions into the film (Donnan exclusion) [93]. Generally, it could be stated that all membranes have a negative charge at the working pH of the MFC in the present study which was kept as 6.30. The negative values also stated the negatively charged surface of membranes which is proof of CEM. The results revealed that membranes have a negative zeta potential under pH > 3.3, which is the isoelectric point (IEP) of the membranes. From Fig. 6, it is clear that if pH goes beyond a specific value, the -TGO incorporated membranes show higher negativity of zeta potential than -SGO membranes. We should also highlight that the zeta potential values of the SPES/SGO1.8% membrane are more negative than SPES/GO1.8% and less negative than SPES/TGO1.8%. The order of membranes in neutral pH is as follows:

SPES/TGO1.2%> SPES/TGO1.8%> SPES/TGO0.6%> SPES> SPES/GO0.6%> SPES/SGO1.2%> SPES/SGO1.8%> SPES/SGO0.6%> SPES/GO1.2%> SPES/GO1.8%

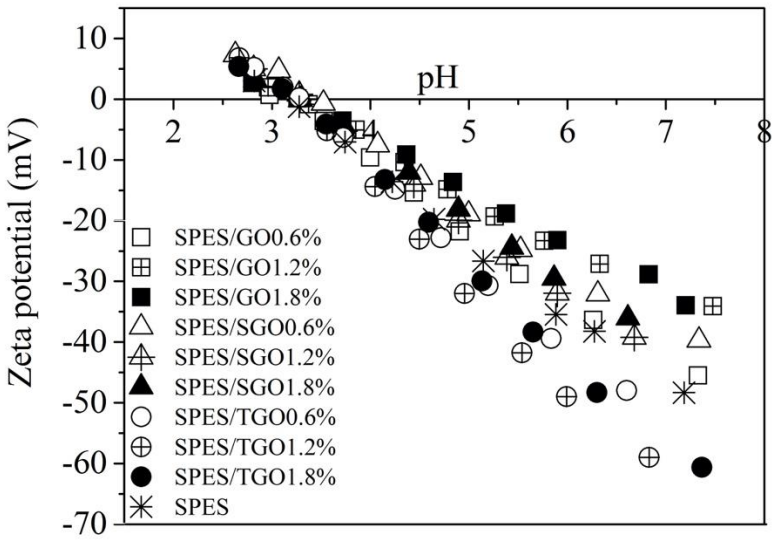

Fig. 6. The zeta potential of membranes in the pH range of 2.5 to 8

3.7. MFC performance

Fig. 7 shows the polarization curves (voltage, current density, and power density) of MFCs working with Nafion117, SPES/GO1.8%, SPES/SGO1.8%, and SPES/TGO1.8% as the separators. The details on P_D and I_D of other membranes are also provided in Table 6. Membranes play important roles in dual-chamber MFCs [5], and their performance is determined by the generated power density. The internal resistance of the MFC is the slope of the I-V curve or in other words, the slope of the current versus the voltage. In this study, the All the MFC reactors had the same configuration and identical substrates. Therefore, the different amounts of power, current, and voltage in systems with different membranes are most likely due to the membranes.

As expected, the highest amount of power density and current density of 66.4 mW/m^2, and 300 mA/m^2 were obtained for SPES/SGO1.8%, followed by SPES/TGO1.8% (54.13mW/m^2, 275 mA/m^2). This amount of power density is almost two times higher than MFC working with Nafion117 (35.9 mW/m^2) and SPES/GO1.8% (39.2 mW/m^2), which is a significant improvement in MFC performance in terms of generating electricity. The efficiency of proposed SPES/SGO1.8% in MFC agrees with the previously provided data as proton conductivity, CEC, WU. The lowest power density and current density are assigned to the

bare SPES membrane as 27.8 mW/m^2 and 216 mA/m^2. These low values of PD for Nafion117 and SPES are because of higher oxygen cross-over through the chamber, which reduces the anaerobic condition for microorganisms [94]. The maximum voltage of about 820 mV was achieved with the system working with SPES/GO1.8%, followed by SPES/TGO1.8%. Nafion117 reached the maximum voltage of 600 mv, which was higher than SPES pure membrane and lower than SPES/GO. It could be observed the addition of functionalized GO has significantly improved the MFC efficiency as generating higher electricity.

Earlier, we have tested SPEEK and SPEEK/GO membranes in MFC [17], where we obtained an almost similar power density for Nafion117 (26 mW/m^2), but a higher amount of power density for SPEEK/GO5% (53.2 mW/m^2) comparing to SPES/GO1.8% (39.2 mW/m^2). This might be derived from the higher ratio of GO in the polymer matrix and the role of SPEEK which is a good choice for PEM. In the current study, we have focused on a more cost-effective and simpler approach by changing the polymer to PES and functionalizing GO. To improve the efficiency of the membrane as CEM, we have sulfonated the polymer [71] (SPES) as well as functionalizing the nanoparticles (TGO and SGO). This resulted in a higher power density and voltage while applying a cheaper polymer and a decrease in usage of nanoparticles to more than half (from 5% in SPEEK/GO to 1.8% in SPES/SGO and SPES/TGO). All these support the idea of proposing a more cost-effective membrane in parallel with better performance.

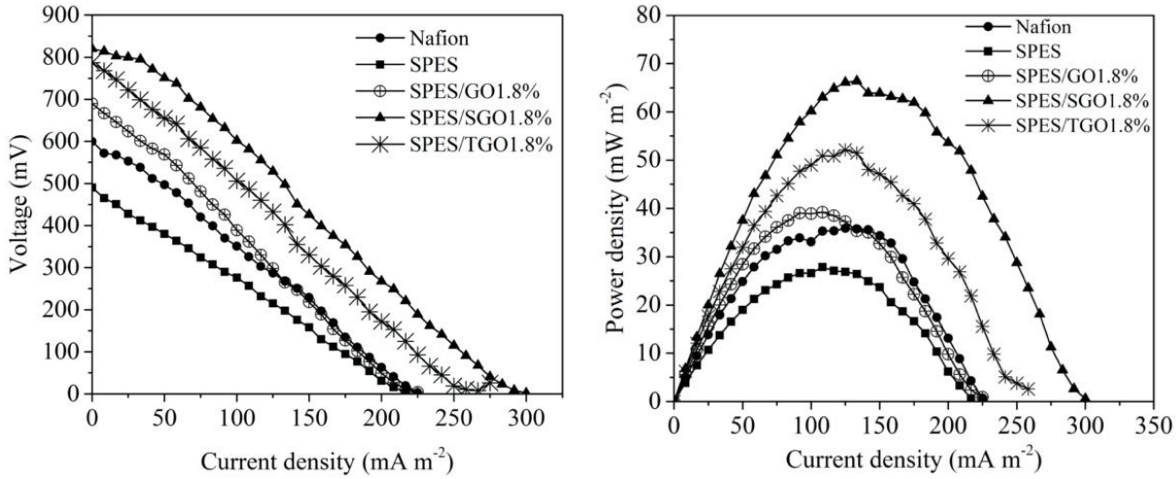

Fig. 7. Polarization curves of MFCs working with membranes: a) voltage versus current density, b) power density versus current density.

The authors have conducted further SEM and AFM analysis of surface morphology and topography on the SPES/SGO1.8% membrane. SPES/SGO1.8% was proved to be the most suitable separator derived from earlier analyses. AFM and SEM images of the membrane surface before and after its application in an MFC are displayed in Fig. 8. The analyses have been conducted after 21 days of exposing the anode compartment. Fig. 8 a shows the surface non-porosity and homogeneity with an average roughness of 41 nm. However, we can easily observe the formation of biofilm (Fig. 8b) and a significant increase in average roughness to a value of 186 nm (Fig. 8d). The biofilm formation may cause a decrease in membrane efficiency in terms of its role on proton transport, thus result in lower MFC performance. The aim of these observations was also to follow the membrane behavior in the presence of biofilm and highlight the importance of emerging further investigation of biofouling studies on newly synthesized membranes.

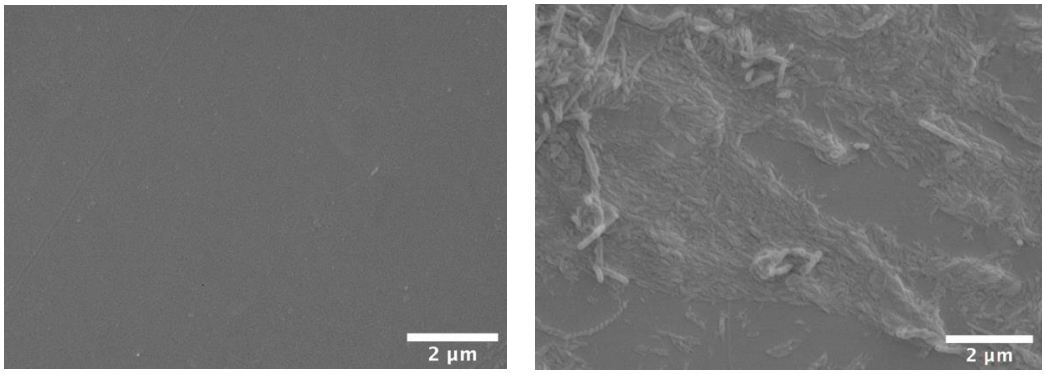

(a) (b)

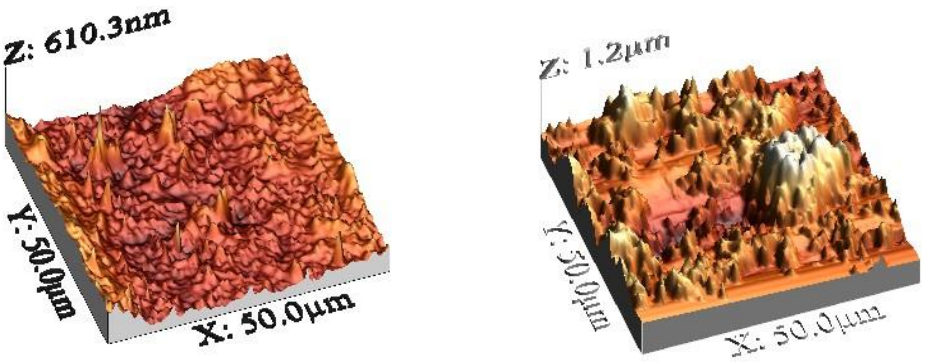

Ave. Ra= 41 nm
RMS = 52.3 nm
(c)

Ave. Ra= 186 nm
RMS = 140 nm
(d)

Fig. 8. Surface image of SPES/SGO1.8% a) side a, b) side b, and AFM images of SPES/SGO1.8% c) side a, d) side b

3.8. COD removal and coulombic efficiency (CE)

The COD removal and CE of MFCs with different membranes are displayed in Table 6. The COD removal percentage did not show a very significant difference in many reactors, and it was high for all the systems (COD>70%). The amounts of COD removal ranged between 72% and 89% for various membranes. The COD removal achieved by Nafion117 was about 82 %, which is higher than SPES (79%), SPES/GO0.6% (75.2%), SPES/GO1.2 % (80.74%), SPES/SGO0.6% (78.21%), and SPES/TGO0.6% (72.53%). The achieved higher COD removal by the system despite the lower power density, is an indication that more substrate was used by microorganisms anaerobically digestion rather than for producing electricity [95]. The highest COD removal and CE were obtained for MFCs working with SPES/SGO1.8% (89.85%, 3.73%), SPES/TGO1.8% (88.07%, 3.2%), respectively, and durability of over 8 days at mid conditions, which indicates the best performances compared to Nafion© -based membrane in MFCs. As discussed above, these alternative membranes showed high power densities compared to commercial Nafion117. The CE values were low in the present study, this is possibly derived from not using any cathode catalyst [95]. The earlier study has compared a PVDF-g-PSSA and Nafion© membrane in an MFC, reporting a

650 low CE of 5% and 7%, respectively. They have well explained that lower CE was due to high
651 substrate concentration and a catalyst-free cathode [61,95].
652
653 **Table 6.** COD removal, Coulombic efficiency, maximum current density, and power density
654 of MFCs working with membranes.

Membrane	COD removal (±5)	CE (±0.2)	$I_D \pm 3$ (mA/m^2)	$P_D \pm 2$ (mW/m^2)
SPES	79.76	2.19	216.7	27.8
SPES/GO0.6%	75.2	2.04	218.7	28.5
SPES/GO1.2%	80.74	2.20	222.1	32.1
SPES/GO1.8%	86.47	2.28	225	39.2
SPES/SGO0.6%	78.21	2.13	233.5	46.8
SPES/SGO1.2%	85.41	2.64	276.4	61.5
SPES/SGO1.8%	89.85	3.73	300	66.4
SPES/TGO0.6%	72.53	2.18	223.6	43.4
SPES/TGO1.2%	85.22	2.51	255	51.7
SPES/TGO1.8%	88.07	3.20	275	54.13
Nafion117	82.71	2.28	233.3	35.9

655
656 **4. Conclusions**
657 Proton exchange membranes have been studied for decades. The role of PEMs in dual-
658 chamber MFCs is more than just a physical separator. These are the key element in
659 transporting the protons from the anode to the cathode compartment completing the cycle of
660 electron transfer, besides avoiding the substrate and oxygen cross-over. There are many
661 commercially available membranes, among which Nafion© is the most usually applied one. It
662 is associated with some limitations that are subject to further studies to overcome those
663 limitations and improve the MFC efficiency. Here, we have developed various membranes
664 using sulfonated polyethersulfone (SPES) combined with GO as well as its sulfonated and
665 thiolated forms (GO, SGO, and TGO). In the second step, we have conducted
666 characterization tests of water uptake, contact angle, zeta potential, oxygen diffusion, proton
667 conductivity, and cation exchange capacity on various prepared membranes and compared
668 the results with Nafion117©. Finally, the membranes were applied in MFC reactors to test
669 their suitability matching the features of electricity generation and bioremediation. Generally,
670 the incorporation of functionalized GO not only improved the water uptake, cation exchange

capacity, oxygen diffusion, contact angle of the composite membranes but also increased their proton conductivities. Broadly translated our findings indicate that SPES/SGO1.8% with proton conductivity of 1.42 mS/cm, water uptake of 36.32%, cation exchange capacity of 0.84 meq/g, and contact angle of 78.5% showed the highest power density of 66.4, COD removal of 90% and CE of 3.73%. the chemical interaction in SPES/SGO and SPES/TGO and the presence of rich functionalized groups of $-SO_3^-$ and -SH, enhance the proton movement via making the channels facilitating the transport. In summary, this paper showed that the SGO nanocomposite membranes achieve the best performance followed by TGO membranes and GO nanocomposite membranes, concluding that the functionalized GO nanocomposite membranes are ideal candidates for utilizing microbial fuel cells. However, Future research should further develop to confirm these initial findings by conducting tests on biofouling of the membranes and application of those proposed membranes in continuous reactors for a longer period of cycles. Besides, implementing anti-biofouling strategies might prove an important area for future research.

Acknowledgments

The authors gratefully acknowledge the financial support of the Iran National Science Foundation (Grant No. 97014305), and the grant support research (IG-39804) of Tarbiat Modares University (TMU). The authors also thank the French embassy in Teheran (Mr. JC Bonté) and campus France for the French/Iranian research Ph.D. (Séréna ALINE) program with funds allocated to Mrs. M. SHABANI, a Ph.D. student from Tarbiat Modares University, Tehran. The authors wish to express their thanks to Romain MALLET and Florence MANERO from Microscopy Dpt (SCIAM) at Angers University, France.

References

[1] B.E. Logan, B. Hamelers, R. Rozendal, U. Schröder, J. Keller, S. Freguia, P. Aelterman, W. Verstraete, K. Rabaey, Microbial Fuel Cells: Methodology and

Technology †, Environ. Sci. Technol. 40 (2006) 5181–5192. doi:10.1021/es0605016.
[2] W. Logroño, M. Pérez, G. Urquizo, A. Kadier, M. Echeverría, C. Recalde, G. Rákhely, Single chamber microbial fuel cell (SCMFC) with a cathodic microalgal biofilm: A preliminary assessment of the generation of bioelectricity and biodegradation of real dye textile wastewater, Chemosphere. (2017). doi:10.1016/j.chemosphere.2017.02.099.
[3] J.M. Sonawane, E. Marsili, P. Chandra Ghosh, Treatment of domestic and distillery wastewater in high surface microbial fuel cells, Int. J. Hydrogen Energy. 39 (2014) 21819–21827. doi:10.1016/j.ijhydene.2014.07.085.
[4] B. Virdis, S. Freguia, R.A. Rozendal, K. Rabaey, Z. Yuan, J. Keller, Microbial Fuel Cells, Hoboken, New Jersey, 2011. doi:10.1016/B978-0-444-53199-5.00098-1.
[5] M. Shabani, H. Younesi, M. Pontié, A. Rahimpour, M. Rahimnejad, A.A. Zinatizadeh, A critical review on recent proton exchange membranes applied in microbial fuel cells for renewable energy recovery, J. Clean. Prod. 264 (2020) 121446. doi:10.1016/j.jclepro.2020.121446.
[6] N.E. Stein, H.V.M.M. Hamelers, C.N.J.J. Buisman, Influence of membrane type, current and potential on the response to chemical toxicants of a microbial fuel cell based biosensor, Sensors Actuators, B Chem. 163 (2012) 1–7. doi:10.1016/j.snb.2011.10.060.
[7] J.X. Leong, W.R.W. Daud, M. Ghasemi, K. Ben Liew, M. Ismail, Ion exchange membranes as separators in microbial fuel cells for bioenergy conversion: A comprehensive review, Renew. Sustain. Energy Rev. 28 (2013) 575–587. doi:10.1016/j.rser.2013.08.052.
[8] X. Zhang, S. Cheng, X. Wang, X. Huang, B.E. Logan, Separator Characteristics for Increasing Performance of Microbial Fuel Cells, Environ. Sci. Technol. 43 (2009) 8456–8461. doi:10.1021/es901631p.
[9] J.R. Kim, S. Cheng, B.E. Logan, J.R.A.E. Kim, S. Cheng, Power Generation Using Different Cation , Anion , and Ultrafiltration Membranes in Microbial Fuel Power Generation Using Different Cation , Anion , and Ultrafiltration Membranes in Microbial Fuel Cells, (2016). doi:10.1021/es062202m.
[10] H.M. Poggi-varaldo, O. Solorza-feria, Electrochimica Acta Use of Novel Reinforced Cation Exchange Membranes for Microbial Fuel Cells, Electrochim. Acta. 176 (2015) 555–566. doi:10.1016/j.electacta.2015.07.042.
[11] S. Ayyaru, S. Dharmalingam, Enhanced response of microbial fuel cell using sulfonated poly ether ether ketone membrane as a biochemical oxygen demand sensor, Anal. Chim. Acta. 818 (2014) 15–22. doi:10.1016/j.aca.2014.01.059.
[12] F.J. Hernández-Fernández, A. Pérez de los Ríos, M.J. Salar-García, V.M. Ortiz-Martínez, L.J. Lozano-Blanco, C. Godínez, F. Tomás-Alonso, J. Quesada-Medina, Recent progress and perspectives in microbial fuel cells for bioenergy generation and wastewater treatment, Fuel Process. Technol. 138 (2015) 284–297. doi:10.1016/j.fuproc.2015.05.022.
[13] G. Hernández-Flores, H.M. Poggi-Varaldo, O. Solorza-Feria, Comparison of alternative membranes to replace high cost Nafion ones in microbial fuel cells, Int. J. Hydrogen Energy. 1 (2016) 2–10. doi:10.1016/j.ijhydene.2016.08.206.
[14] K.A. Mauritz, R.B. Moore, State of Understanding of Nafion, Chem. Rev. 104 (2004) 4535–4586. doi:10.1021/cr0207123.
[15] K. Gaurav, R. Singh, B.K. Tiwari, R. Srivastava, Novel proton exchange membranes based on PVC for microbial fuel cells (MFCs), J. Polym. Eng. 39 (2019) 360–367. doi:10.1515/polyeng-2018-0276.
[16] A.A. Olayiwola Sirajudeen, M.S. Mohamad Annuar, K.A. Ishak, H. Yusuf, R. Subramaniam, Innovative application of biopolymer composite as proton exchange

membrane in microbial fuel cell utilizing real wastewater for electricity generation, J. Clean. Prod. 278 (2021) 123449. doi:10.1016/j.jclepro.2020.123449.
[17] M. Shabani, H. Younesi, A. Rahimpour, M. Rahimnejad, Upgrading the electrochemical performance of graphene oxide-blended sulfonated polyetheretherketone composite polymer electrolyte membrane for microbial fuel cell application, Biocatal. Agric. Biotechnol. 22 (2019) 101369. doi:10.1016/j.bcab.2019.101369.
[18] A.H. Avci, T. Rijnaarts, E. Fontananova, G. Di Profio, I.F. V Vankelecom, W.M. De Vos, E. Curcio, Sulfonated polyethersulfone based cation exchange membranes for reverse electrodialysis under high salinity gradients, J. Memb. Sci. 595 (2020) 117585. doi:10.1016/j.memsci.2019.117585.
[19] K. Widhyahrini, N. Handayani, D. Wahyuningrum, C.L. Radiman, The synthesis of sulfonated polyethersulfone (SPES) and the preparation of its membranes as matrix in the immobilization of Candida antarctica lipase B (Cal-B), Polym. Bull. 77 (2020) 3735–3748. doi:10.1007/s00289-019-02932-7.
[20] A. Kraytsberg, Y. Ein-Eli, Review of Advanced Materials for Proton Exchange Membrane Fuel Cells, Energy & Fuels. 28 (2014) 7303–7330. doi:10.1021/ef501977k.
[21] S.S. Lim, W.R.W. Daud, J. Md Jahim, M. Ghasemi, P.S. Chong, M. Ismail, S. Su, W. Ramli, W.R.W. Daud, J. Jahim, M. Ghasemi, S.S. Lim, W.R.W. Daud, J. Md Jahim, M. Ghasemi, P.S. Chong, M. Ismail, Sulfonated poly(ether ether ketone)/poly(ether sulfone) composite membranes as an alternative proton exchange membrane in microbial fuel cells, Int. J. Hydrogen Energy. 37 (2012) 11409–11424. doi:10.1016/j.ijhydene.2012.04.155.
[22] V. Kumar, S. Mondal, A. Nandy, P.P. Kundu, Analysis of polybenzimidazole and polyvinylpyrrolidone blend membranes as separating barrier in single chambered microbial fuel cells, Biochem. Eng. J. 111 (2016) 34–42. doi:10.1016/j.bej.2016.03.003.
[23] K. Noel Jacob, S. Senthil Kumar, A. Thanigaivelan, M. Tarun, D. Mohan, Sulfonated polyethersulfone-based membranes for metal ion removal via a hybrid process, J. Mater. Sci. 49 (2014) 114–122. doi:10.1007/s10853-013-7682-1.
[24] P.N. Venkatesan, S. Dharmalingam, Effect of cation transport of SPEEK – Rutile TiO2 electrolyte on microbial fuel cell performance, J. Memb. Sci. 492 (2015) 518–527. doi:10.1016/j.memsci.2015.06.025.
[25] Q. Xu, L. Wang, C. Li, X. Wang, C. Li, Y. Geng, Study on improvement of the proton conductivity and anti-fouling of proton exchange membrane by doping SGO@SiO_2 in microbial fuel cell applications, Int. J. Hydrogen Energy. 44 (2019) 15322–15332. doi:10.1016/j.ijhydene.2019.03.238.
[26] H. Beydaghi, M. Javanbakht, E. Kowsari, Preparation and physicochemical performance study of proton exchange membranes based on phenyl sulfonated graphene oxide nanosheets decorated with iron titanate nanoparticles, Polymer (Guildf). 87 (2016) 26–37. doi:10.1016/j.polymer.2016.01.068.
[27] T. Tavangar, A. Hemmati, M. Karimi, Layer - by - layer assembly of graphene oxide (GO) on sulfonated polyethersulfone (SPES) substrate for effective dye removal, Polym. Bull. 76 (2019) 35–52. doi:10.1007/s00289-018-2357-3.
[28] A. Muthumeenal, M.S.A. Saraswathi, D. Rana, A. Nagendran, Fabrication and electrochemical properties of highly selective SPES/GO composite membranes for direct methanol fuel cells, J. Environ. Chem. Eng. 5 (2017) 3828–3833. doi:10.1016/j.jece.2017.07.036.
[29] B. Roshanravan, H. Younesi, M. Abdollahi, M. Rahimnejad, S.H. Pyo, Application of proton-conducting sulfonated polysulfone incorporated MIL-100(Fe) composite materials for polymer-electrolyte membrane microbial fuel cells, J. Clean. Prod. 300

(2021) 126963. doi:10.1016/j.jclepro.2021.126963.
[30] K. Kim, J. Bae, M.Y. Lim, P. Heo, S.W. Choi, H.H. Kwon, J.C. Lee, Enhanced physical stability and chemical durability of sulfonated poly(arylene ether sulfone) composite membranes having antioxidant grafted graphene oxide for polymer electrolyte membrane fuel cell applications, J. Memb. Sci. 525 (2017) 125–134. doi:10.1016/j.memsci.2016.10.038.
[31] M. Yun, M.S. Ahmed, S. Jeon, Thiolated graphene oxide-supported palladium cobalt alloyed nanoparticles as high performance electrocatalyst for oxygen reduction reaction, J. Power Sources. 293 (2015) 380–387. doi:10.1016/j.jpowsour.2015.05.094.
[32] A.N. Nikam, M.P. More, A.P. Pandey, P.O. Patil, A.G. Patil, P.K. Deshmukh, Design and development of thiolated graphene oxide nanosheets for brain tumor targeting, Int. J. Polym. Mater. Polym. Biomater. 69 (2020) 611–621. doi:10.1080/00914037.2019.1596911.
[33] J. Debgupta, V.K. Pillai, Thiolated graphene-a new platform for anchoring CdSe quantum dots for hybrid heterostructures, Nanoscale. 5 (2013) 3615–3619. doi:10.1039/c3nr00363a.
[34] K. Gerani, H.R. Mortaheb, B. Mokhtarani, Enhancement in Performance of Sulfonated PES Cation-Exchange Membrane by Introducing Pristine and Sulfonated Graphene Oxide Nanosheets Synthesized through Hummers and Staudenmaier Methods, Polym. - Plast. Technol. Eng. 56 (2017) 543–555. doi:10.1080/03602559.2016.1233260.
[35] E. Mohammadnia, M. Hadavifar, H. Veisi, Kinetics and thermodynamics of mercury adsorption onto thiolated graphene oxide nanoparticles, Polyhedron. 173 (2019) 114139. doi:10.1016/j.poly.2019.114139.
[36] T. Tavangar, A. Hemmati, M. Karimi, F. Zokaee Ashtiani, Layer-by-layer assembly of graphene oxide (GO) on sulfonated polyethersulfone (SPES) substrate for effective dye removal, Polym. Bull. 76 (2019) 35–52. doi:10.1007/s00289-018-2357-3.
[37] A.K. Mishra, N.H. Kim, D. Jung, J.H. Lee, Enhanced mechanical properties and proton conductivity of Nafion-SPEEK-GO composite membranes for fuel cell applications, J. Memb. Sci. 458 (2014) 128–135. doi:10.1016/j.memsci.2014.01.073.
[38] P. Bunlengsuwan, N. Paradee, A. Sirivat, Influence of Sulfonated Graphene Oxide on Sulfonated Polysulfone Membrane for Direct Methanol Fuel Cell, Polym. - Plast. Technol. Eng. 56 (2017) 1695–1703. doi:10.1080/03602559.2017.1289398.
[39] H. Wu, Y. Fu, C. Guo, Y. Li, N. Jiang, C. Yin, Electricity generation and removal performance of a microbial fuel cell using sulfonated poly (ether ether ketone) as proton exchange membrane to treat phenol/acetone wastewater, Bioresour. Technol. 260 (2018) 130–134. doi:10.1016/j.biortech.2018.03.133.
[40] X. Qiu, T. Dong, M. Ueda, X. Zhang, L. Wang, Sulfonated reduced graphene oxide as a conductive layer in sulfonated poly (ether ether ketone) nanocomposite membranes, J. Memb. Sci. 524 (2017) 663–672. doi:10.1016/j.memsci.2016.11.064.
[41] N. Cao, C. Zhou, Y. Wang, H. Ju, D. Tan, J. Li, Synthesis and characterization of sulfonated graphene oxide reinforced sulfonated poly (ether ether ketone) (SPEEK) composites for proton exchange membrane materials, Materials (Basel). 11 (2018) 516. doi:10.3390/ma11040516.
[42] H. Lee, J. Han, K. Kim, J. Kim, E. Kim, H. Shin, J.C. Lee, Highly sulfonated polymer-grafted graphene oxide composite membranes for proton exchange membrane fuel cells, J. Ind. Eng. Chem. 74 (2019) 223–232. doi:10.1016/j.jiec.2019.03.012.
[43] C. V. Pham, M. Eck, M. Krueger, C. V. Pham, M. Eck, M. Krueger, Thiol functionalized reduced graphene oxide as a base material for novel graphene-nanoparticle hybrid composites, Chem. Eng. J. 231 (2013) 146–154. doi:10.1016/j.cej.2013.07.007.
[44] Y. Liu, Y. Liu, Z. Meng, Y. Qin, D. Jiang, K. Xi, P. Wang, Thiol-functionalized

reduced graphene oxide as self-assembled ion-to-electron transducer for durable solid-contact ion-selective electrodes, Talanta. 208 (2020) 120374. doi:10.1016/j.talanta.2019.120374.
[45] R. Guan, H. Zou, D. Lu, C. Gong, Y. Liu, Polyethersulfone sulfonated by chlorosulfonic acid and its membrane characteristics, Eur. Polym. J. 41 (2005) 1554–1560. doi:10.1016/j.eurpolymj.2005.01.018.
[46] W.S. Hummers, R.E. Offeman, Preparation of Graphitic Oxide, J. Am. Chem. Soc. 80 (1958) 1339–1339. doi:10.1021/ja01539a017.
[47] M. Macchione, J.C. Jansen, E. Drioli, The dry phase inversion technique as a tool to produce highly efficient asymmetric gas separation membranes of modified PEEK. Influence of temperature and air circulation, Desalination. 192 (2006) 132–141. doi:10.1016/j.desal.2005.09.020.
[48] H. Strathmann, A. Grabowski, G. Eigenberger, Ion-Exchange Membranes in the Chemical Process Industry, Ind. Eng. Chem. Res. 52 (2013) 10364–10379. doi:10.1021/ie4002102.
[49] M. Pontié, H. Dach, J. Leparc, M. Hafsi, A. Lhassani, Novel approach combining physico-chemical characterizations and mass transfer modelling of nanofiltration and low pressure reverse osmosis membranes for brackish water desalination intensification, Desalination. 221 (2008) 174–191.
[50] R.S.L. Yee, K. Zhang, B.P. Ladewig, The effects of sulfonated poly(ether ether ketone) ion exchange preparation conditions on membrane properties, Membranes (Basel). 3 (2013) 182–195. doi:10.3390/membranes3030182.
[51] Q. Duan, S. Ge, C.Y. Wang, Water uptake, ionic conductivity and swelling properties of anion-exchange membrane, J. Power Sources. 243 (2013) 773–778. doi:10.1016/j.jpowsour.2013.06.095.
[52] W.R.W. Daud, M. Ghasemi, P.S. Chong, J.M. Jahim, S.S. Lim, M. Ismail, SPEEK/PES composite membranes as an alternative for proton exchange membrane in microbial fuel cell (MFC), in: 2011 IEEE 1st Conf. Clean Energy Technol. CET 2011, IEEE, 2011: pp. 400–403. doi:10.1109/CET.2011.6041505.
[53] M. Saito, N. Arimura, K. Hayamizu, T. Okada, Mechanisms of ion and water transport in perfluorosulfonated ionomer membranes for fuel cells, J. Phys. Chem. B. 108 (2004) 16064–16070. doi:10.1021/jp0482565.
[54] V. Tourreuil, N. Rossignol, G. Bulvestre, C. Larchet, B. Auclair, Détermination de la séléctivité d'une membrane échangeuse d'ions: confrontation entre le flux de diffusion et le nombre de transport, Eur. Polym. J. 34 (1998) 1415–1421. doi:10.1016/S0014-3057(97)00288-7.
[55] J.O. Bockris, A.K.N. Reddy, Modern Electrochemistry 1, Kluwer Academic Publishers, Boston, 2002. doi:10.1007/b114546.
[56] P. Fievet, B. Aoubiza, A. Szymczyk, J. Pagetti, Membrane potential in charged porous membranes, J. Memb. Sci. 160 (1999) 267–275.
[57] R. Gaboriaud, Thermodynamique appliquée à la chimie des solutions, Ellipses, 1988.
[58] P. Fievet, M. Sbaï, A. Szymczyk, C. Magnenet, C. Labbez, A. Vidonne, A new tangential streaming potential setup for the electrokinetic characterization of tubular membranes, Sep. Sci. Technol. 39 (2004) 2931–2949.
[59] P. Fievet, M. Sbai, A. Szymczyk, Analysis of the pressure-induced potential arising across selective multilayer membranes, J. Memb. Sci. 264 (2005) 1–12.
[60] Q. Liao, J. Zhang, J. Li, D. Ye, X. Zhu, J. Zheng, B. Zhang, Electricity generation and COD removal of microbial fuel cells (MFCs) operated with alkaline substrates, Int. J. Hydrogen Energy. 39 (2014) 19349–19354. doi:10.1016/j.ijhydene.2014.06.058.
[61] J. Heilmann, B.E. Logan, Production of Electricity from Proteins Using a Microbial Fuel Cell, Water Environ. Res. 78 (2006) 531–537. doi:10.2175/106143005X73046.

[62] M. Yari, M. Rajabi, O. Moradi, A. Yari, M. Asif, S. Agarwal, V.K. Gupta, Kinetics of the adsorption of Pb(II) ions from aqueous solutions by graphene oxide and thiol functionalized graphene oxide, J. Mol. Liq. 209 (2015) 50–57. doi:10.1016/j.molliq.2015.05.022.
[63] S. Neelakandan, K. Noel Jacob, P. Kanagaraj, R.M. Sabarathinam, A. Muthumeenal, A. Nagendran, Effect of sulfonated graphene oxide on the performance enhancement of acid-base composite membranes for direct methanol fuel cells, RSC Adv. 6 (2016) 51599–51608. doi:10.1039/c5ra27655a.
[64] M.H. Gouda, W. Gouveia, M.L. Afonso, B. Šljukić, N.A. El Essawy, A.B.A.A. Nassr, D.M.F. Santos, Poly(vinyl alcohol)-based crosslinked ternary polymer blend doped with sulfonated graphene oxide as a sustainable composite membrane for direct borohydride fuel cells, J. Power Sources. 432 (2019) 92–101. doi:10.1016/j.jpowsour.2019.05.078.
[65] E.S. Orth, J.E.S. Fonsaca, S.H. Domingues, H. Mehl, M.M. Oliveira, A.J.G. Zarbin, Targeted thiolation of graphene oxide and its utilization as precursor for graphene/silver nanoparticles composites, Carbon N. Y. 61 (2013) 543–550. doi:10.1016/j.carbon.2013.05.032.
[66] S. Gahlot, P.P. Sharma, V. Kulshrestha, P.K. Jha, SGO/SPES-based highly conducting polymer electrolyte membranes for fuel cell application, ACS Appl. Mater. Interfaces. 6 (2014) 5595–5601. doi:10.1021/am5000504.
[67] H. Beydaghi, M. Javanbakht, E. Kowsari, Synthesis and characterization of poly(vinyl alcohol)/Sulfonated graphene oxide nanocomposite membranes for use in proton exchange membrane fuel cells (PEMFCs), Ind. Eng. Chem. Res. 53 (2014) 16621–16632. doi:10.1021/ie502491d.
[68] N. Oger, Y.F. Lin, C. Labrugère, E. Le Grognec, F. Rataboul, F.X. Felpin, Practical and scalable synthesis of sulfonated graphene, Carbon N. Y. 96 (2016) 342–350. doi:10.1016/j.carbon.2015.09.082.
[69] A.B. Shivanandareddy, M. Kumar, V. Lakshminarayanan, S. Kumar, Self-assembly of thiolated graphene oxide onto a gold surface and in the supramolecular order of discotic liquid crystals, RSC Adv. 5 (2015) 47692–47700. doi:10.1039/c5ra06713h.
[70] L.F. Greenlee, N.S. Rentz, R.E. Martin, Influence of nanoparticle processing and additives on PES casting solution viscosity and cast membrane characteristics, Polymer (Guildf). 103 (2016) 498–508. doi:10.1016/j.polymer.2016.04.021.
[71] C. Klaysom, B.P. Ladewig, G.Q.M. Lu, L. Wang, Preparation and characterization of sulfonated polyethersulfone for cation-exchange membranes, J. Memb. Sci. 368 (2011) 48–53. doi:10.1016/j.memsci.2010.11.006.
[72] F. Wang, M. Hickner, Y.S. Kim, T.A. Zawodzinski, J.E. McGrath, Direct polymerization of sulfonated poly(arylene ether sulfone) random (statistical) copolymers: Candidates for new proton exchange membranes, J. Memb. Sci. 197 (2002) 231–242. doi:10.1016/S0376-7388(01)00620-2.
[73] H. Nagar, N. Badhrachalam, V.V.B. Rao, S. Sridhar, A novel microbial fuel cell incorporated with polyvinylchloride/4A zeolite composite membrane for kitchen wastewater reclamation and power generation, Mater. Chem. Phys. 224 (2019) 175–185. doi:10.1016/J.MATCHEMPHYS.2018.12.023.
[74] S. Angioni, L. Millia, G. Bruni, D. Ravelli, P. Mustarelli, E. Quartarone, Novel composite polybenzimidazole-based proton exchange membranes as efficient and sustainable separators for microbial fuel cells, J. Power Sources. 348 (2017) 57–65. doi:10.1016/j.jpowsour.2017.02.084.
[75] D. Li, J. Wu, S. Yang, W. Zhang, F. Ran, Hydrophilicity and anti-fouling modification of polyethersulfone membrane by grafting copolymer chains: Via surface initiated electrochemically mediated atom transfer radical polymerization, New J. Chem. 41

(2017) 9918–9930. doi:10.1039/c7nj01825h.
[76] M. Oliot, S. Galier, H. Roux de Balmann, A. Bergel, Ion transport in microbial fuel cells: Key roles, theory and critical review, Appl. Energy. 183 (2016) 1682–1704. doi:10.1016/j.apenergy.2016.09.043.
[77] W.W. Li, G.P. Sheng, X.W. Liu, H.Q. Yu, Recent advances in the separators for microbial fuel cells, Bioresour. Technol. 102 (2011) 244–252. doi:10.1016/j.biortech.2010.03.090.
[78] R. Lteif, L. Dammak, C. Larchet, B. Auclair, Determination du nombre de transport d'un contre-ion dans une membrane echangeuse d'ions en utilisant la methode de la pile de concentration, Eur. Polym. J. 37 (2001) 627–639. doi:10.1016/S0014-3057(00)00163-4.
[79] Y. Kimura, H.-J. Lim, T. Iijima, Permeability of alkali chlorides through charged cellulosic membranes, Angew. Makromol. Chemie. 138 (1986) 151–158. doi:10.1002/apmc.1986.051380112.
[80] G.M. Geise, B.D. Freeman, D.R. Paul, Characterization of a sulfonated pentablock copolymer for desalination applications, Polymer (Guildf). 51 (2010) 5815–5822. doi:10.1016/j.polymer.2010.09.072.
[81] W.G. Sunu, D.N. Bennion, Relative Transport Rates of Alkali Ions across Modified Cellulose Acetate Membranes, Ind. Eng. Chem. Fundam. 16 (1977) 283–289. doi:10.1021/i160062a019.
[82] Y.H. Cho, H.W. Kim, H.D. Lee, J.E. Shin, B.M. Yoo, H.B. Park, Water and ion sorption, diffusion, and transport in graphene oxide membranes revisited, J. Memb. Sci. 544 (2017) 425–435. doi:10.1016/j.memsci.2017.09.043.
[83] K. Ben Liew, J.X. Leong, W.R. Wan Daud, A. Ahmad, J.J. Hwang, W. Wu, Incorporation of silver graphene oxide and graphene oxide nanoparticles in sulfonated polyether ether ketone membrane for power generation in microbial fuel cell, J. Power Sources. 449 (2020) 227490. doi:10.1016/j.jpowsour.2019.227490.
[84] D.P. Wilkinson, J. Zhang, R. Hui, J. Fergus, X. Li, Proton exchange membrane fuel cells: Materials properties and performance, CRC press, 2009.
[85] D.Y. Kwok, A.W. Neumann, Contact angle measurement and contact angle interpretation, Adv. Colloid Interface Sci. 81 (1999) 167–249. doi:10.1016/S0001-8686(98)00087-6.
[86] J.D. Eick, R.J. Good, A.W. Neumann, Thermodynamics of contact angles. II. Rough solid surfaces, J. Colloid Interface Sci. 53 (1975) 235–248. doi:10.1016/0021-9797(75)90010-7.
[87] H. Dach, Comparison of nanofiltration and reverse osmosis processes for a selective desalination of brackish water feeds, Université d'Angers, 2008. https://tel.archives-ouvertes.fr/tel-00433513.
[88] W. Zhao, Q. Mou, X. Zhang, J. Shi, S. Sun, C. Zhao, Preparation and characterization of sulfonated polyethersulfone membranes by a facile approach, Eur. Polym. J. 49 (2013) 738–751. doi:10.1016/j.eurpolymj.2012.11.018.
[89] S. Zinadini, A.A. Zinatizadeh, M. Rahimi, V. Vatanpour, Z. Rahimi, High power generation and COD removal in a microbial fuel cell operated by a novel sulfonated PES/PES blend proton exchange membrane, Energy. 125 (2017) 427–438. doi:10.1016/j.energy.2017.02.146.
[90] H.N. Yang, W.H. Lee, B.S. Choi, W.J. Kim, Preparation of Nafion/Pt-containing TiO2/graphene oxide composite membranes for self-humidifying proton exchange membrane fuel cell, J. Memb. Sci. 504 (2016) 20–28. doi:10.1016/j.memsci.2015.12.021.
[91] K. Reid, M. Dixon, C. Pelekani, K. Jarvis, M. Willis, Y. Yu, Biofouling control by hydrophilic surface modification of polypropylene feed spacers by plasma

polymerisation, Desalination. 335 (2014) 108–118. doi:10.1016/j.desal.2013.12.017.
[92] J. Lee, H.R. Chae, Y.J. Won, K. Lee, C.H. Lee, H.H. Lee, I.C. Kim, J. min Lee, Graphene oxide nanoplatelets composite membrane with hydrophilic and antifouling properties for wastewater treatment, J. Memb. Sci. 448 (2013) 223–230. doi:10.1016/j.memsci.2013.08.017.
[93] M. Adusumilli, M.L. Bruening, Variation of ion-exchange capacity, ζ potential, and ion-transport selectivities with the number of layers in a multilayer polyelectrolyte film, Langmuir. 25 (2009) 7478–7485. doi:10.1021/la900391q.
[94] P. Narayanaswamy Venkatesan, S. Dharmalingam, Characterization and performance study on chitosan-functionalized multi walled carbon nano tube as separator in microbial fuel cell, J. Memb. Sci. 435 (2013) 92–98. doi:10.1016/j.memsci.2013.01.064.
[95] C. Li, L. Wang, X. Wang, M. Kong, Q. Zhang, G. Li, Synthesis of PVDF-g-PSSA proton exchange membrane by ozone-induced graft copolymerization and its application in microbial fuel cells, J. Memb. Sci. 527 (2017) 35–42. doi:10.1016/j.memsci.2016.12.065.